Dynamics of a memristor-meminductor-based chaotic system

DANIEL MONTESINOS CAPACETE[1]

[1] *Master Student in Physics of Complex Systems*

February 16, 2024

Memristors, memcapacitors, and meminductors have gained significant interest for their potential applications in memory devices, artificial neural networks, logic circuits, and nonlinear circuits. These elements store information based on their state and history without requiring a continuous power supply. In this study, we aim to reproduce and investigate the complex dynamical behaviors of a memristor-meminductor-based chaotic system, as presented in [1]. By analyzing chaotic, bursting, and quasi-periodic phenomena in the system under various parameter settings and initial conditions, we seek to gain deeper insights into its underlying dynamics. All the scripts that we will use in this study are available at [2].

1. INTRODUCTION

The memristor, initially conceptualized by Chua [3] and further defined by Chua and Kang in 1976 [4], gained substantial interest following its physical realization by Hewlett-Packard laboratories in 2008 [5]. Chua et al. expanded the concept of memory devices beyond memristors to include memcapacitors and meminductors, which exhibit hysteretic loops in their respective constitutive variables [6]. These memory elements store information based on their state and history without requiring a continuous power supply, this is, they are capable of maintaining their stored data even when the power source is removed (nonvolatile memory devices). Mathematical models and equivalent circuits for meminductors have been developed, including flux-controlled meminductors [7] and floating meminductor emulators [8].

Together, memristors, memcapacitors, and meminductors serve as memory elements applicable in various fields such as nonvolatile memory [6], artificial neural networks [9], logic circuits [10], and nonlinear circuits [11]. Memristive synapses have been use to enhance neuron models and implemented memristor-based neural networks for machine learning tasks [12]. Additionally, memristor-based networks, such as fully convolutional networks and echo state networks, have demonstrated promising results in tasks such as image segmentation and power load forecasting [13, 14].

The field of these memory elements is growing fast and have applications in a wide variety of fields as we have seen. Our aim is to reproduce some of the results in [1] in which a memristor-meminductor-based chaotic system is presented. This circuit is just a memristor, meminductor, capacitor parallel circuit that possesses complex dynamical behaviors, such as bursting, transient phenomenon, intermittency and coexisting attractors as shown in [1].

2. DEFINING THE MODEL

Chua and Kang provided the following general definition for a memristor system [4]:

$$z(t) = G(x, y, t)x(t), \quad \dot{y}(t) = F(x, y, t) \tag{2.1}$$

where $x(t)$, $z(t)$, $y(t)$ are the input, output and state variable of the memristor respectively. The functions $G(x, y, t)$ and $F(x, y, t)$ depend on the specific memristor. Following [1], we are going to be using a voltage-controlled memristor given by

$$i_M = (Ay^2 - B)v_M, \quad \dot{y}(t) = -cv_M - dy + ev_M^2 y \tag{2.2}$$

where i_M and v_M refers to the current and voltage across the memristor and A, B, c, d and e are constants that are related to resistances and capacities in the circuit as can be seen in [1].

On the other hand, a flux-controlled meminductor system is defined by [6]

$$i_{LM} = L^{-1}(\rho)\psi, \quad \dot{\rho} = \psi \tag{2.3}$$

where ψ is the flux, i_{LM} is the output intensity and ρ is the state variable of the meminductor. Following [1], we will be using

$$i_{LM} = (A' + B'\rho)\psi, \quad \dot{\rho} = \psi \tag{2.4}$$

where A' and B' are also constants that are related to resistances in the circuit. The specific details regarding the

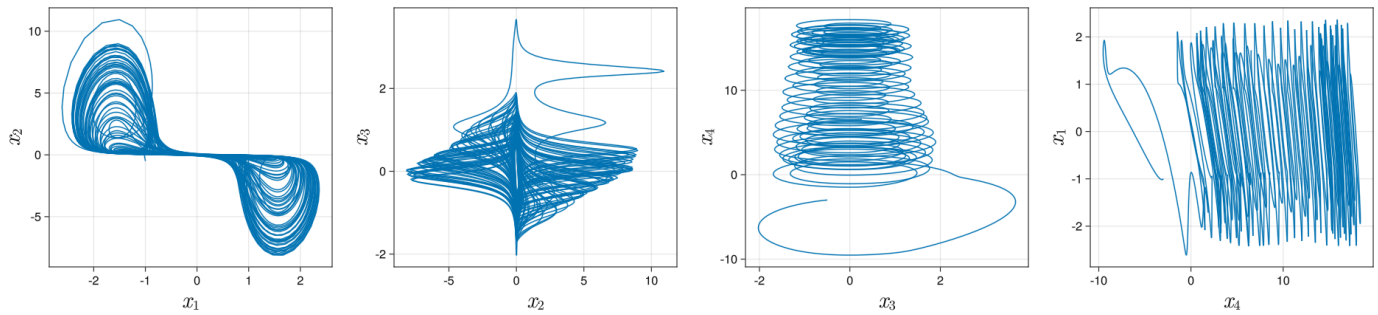

Fig. 2.1. The images show the chaotic attractor of the system. Each of the four pictures illustrates the projection of different variables within the system. From left to right, the images display the x_1-x_2, x_2-x_3, x_3-x_4, and x_4-x_1 phase portraits. This behavior is in accordance with the one shown in [1] for the parameters that are being used.

values of the constants and the circuit's shape are provided in [1].

Both systems possess memory, meaning they can retain information about past conditions even after those conditions have changed or stopped. This ability to remember past states is due to the fundamental properties of these devices and how they react to changes in electrical factors such as voltage or magnetic flux. For meminductors, this memory is tied to the magnetic flux that has passed through them in the past, affecting their inductance not only at the present moment but also reflecting previous flux conditions. Something similar occurs in the memristor with the corresponding voltage.

In [1], a three-element circuit using the previously discussed memristor and meminductor models, along with a capacitor, is proposed. The dynamical system obtained from this circuit is

$$\begin{cases} \dot{x}_1 = -\left(ax_2^2 - b\right) x_1 - (\alpha x_4 + \beta) x_3, \\ \dot{x}_2 = -cx_1 - dx_2 + ex_1^2 x_2, \\ \dot{x}_3 = x_1, \\ \dot{x}_4 = x_3 \end{cases} \tag{2.5}$$

where x_1, x_2, x_3, x_4 relates to the voltage across the capacitor v_C, the state variable $y(t)$ of the memristor, the flux ψ of the meminductor and its state variable ρ respectively. The parameters of the system are a, b, c, d, e, α and β. In the upcoming sections, we will explore the behavior of this 4D system.

3. NUMERICAL DETAILS

To integrate the system of coupled differential equations described by Equation 2.5, we will use the DynamicalSystems.jl package, a Julia software library designed for nonlinear dynamics and nonlinear time series analysis [15]. Specifically, we will employ the Tsit5 algorithm from the DifferentialEquations.jl Julia package [16], which is a fifth-order explicit Runge-Kutta method with an embedded error estimator developed by Tsitouras in 2011 [17]. The integration time step will be set to $\Delta t = 0.001$. Note that in [1], there is no information about the numerical methods that are being used.

In order to calculate the Lyapunov exponents of the system, we will use the *lyapunovspectrum* function from ChaosTools.jl which is a package that is contained within the DynamicalSystems.jl library. This function calculates the spectrum of Lyapunov exponents by applying a QR-decomposition on the parallelepiped defined by the deviation vectors, in total for N evolution steps [18]. We will be using a transient time of 100 time units. Determining whether a Lyapunov exponent can be considered zero or not is a tricky task because the exact values will slightly depend on the specific value of N. In order to address this problem, I calculated the Lyapunov spectrum for $N = 10^3$, 10^4, and 10^5 for a value of the parameters which is known to be non chaotic. While doing this, I noticed some slight changes in all the values of the Lyapunov exponents, but notably, the first exponent dropped from about 10^{-3} to around 10^{-5} as N increased. So, the criteria that I will be using is that if a Lyapunov exponent is around 10^{-5} or smaller, we can consider it zero. For all the Lyapunov exponents that I will compute, I am going to use $N = 10^5$.

4. RESULTS

4.1. Chaotic Behaviour

In this section, we are going to be using $a = 0.1$, $b = 0.5$, $c = 0.5$, $d = 10$, $e = 4.0$, $\alpha = 0.1$ and $\beta = 1.0$. As initial condition, we will use $\vec{x}_0 = (-1, -0.5, -0.5, -3)$. These are the same parameters and initial condition that are used in [1]. The first thing that we can notice is that the divergence of the system is given by

$$\nabla \cdot \dot{\vec{x}} = \sum_{i=1}^{4} \frac{\partial \dot{x}_i}{\partial x_i} = -ax_2^2 + b - d + ex_1^2. \tag{4.1}$$

With the parameters and initial condition that we are using we have that the divergences is negative so the system is dissipative. This is similar to what happens in the Lorenz system which is also dissipative. Thus, it may be possible to find chaotic behavior in our system. However,

it is worth noting that depending on the values of x_1, this divergence could also be positive. We will see in the simulations that the value of x_1 usually falls approximately within the interval $[-2.5, 2.5]$. Therefore, with the parameters that we are using, it is unlikely that the divergence becomes positive. The result for numerically simulating these equations can be seen at Fig. 2.1. We will later discuss more details in order to properly address the chaotic behaviour.

First, we will perform a simple linear stability analysis. Looking at Ec. 2.5, it is straight forward to see that there exists a line of fixed points given by $(0, 0, 0, x_4)\ \forall x_4 \in \mathbb{R}$. The Jacobian matrix of the system evaluated in the fixed points is

$$\mathrm{J} = \begin{pmatrix} b & 0 & -(\alpha x_4 + \beta) & 0 \\ -c & -d & 0 & 0 \\ 1 & 0 & 0 & 0 \\ 0 & 0 & 1 & 0 \end{pmatrix}, \tag{4.2}$$

Using this matrix, the following characteristic equation for the eigenvalues can be obtained:

$$\lambda[\lambda^3 + (d-b)\lambda^2 + (\alpha x_4 + \beta - bd)\lambda + d(\alpha x_4 + \beta)] = 0 \tag{4.3}$$

We have a straightforward solution with $\lambda_0 = 0$, while the remaining solutions are derived from a cubic equation. By numerically solving this cubic equation using the predetermined parameters and initial conditions, we can obtain the following solutions:

$$\lambda_0 = 0, \quad \lambda_1 = -10, \quad \lambda_{2,\pm} = 0.2500 \pm 0.7984i. \tag{4.4}$$

The numerical solution for the cubic is obtained using the Polynomials.jl Julia package. Examining the eigenvalues, we determine that the fixed points form an unstable saddle-focus line. Specifically, we identify a direction where perturbations do not amplify ($\lambda_0 = 0, \ \lambda_1 = -10$), while in two other eigendirections, the fixed points exhibit unstable focus behavior ($\lambda_{2,\pm} = 0.2500 \pm 0.7984i$). Computing the Lyapunov spectrum for this scenario we find $\mathrm{LE}_1 = 0.0672$, $\mathrm{LE}_2 = 0$, $\mathrm{LE}_3 = -0.08285$ and $\mathrm{LE}_4 = -4.1656$. Since we have a positive Lyapunov exponent, the system exhibits chaotic dynamics. To illustrate this, in the video file "x1x2x3_3D.mp4", you can observe these dynamics with three initial conditions that are slightly modified versions of the one we previously defined, with a small change of 10^{-4}. In the video, we can observe how all three slightly different initial conditions exhibit completely different behaviors as time progresses.

4.2. Influence of the Parameters

In this section, we aim to study how the dynamics of Eq. 2.5 changes with parameter a. In order to to that, we will compute the Lyapunov spectrum and the corresponding bifurcation diagram as a function of the parameter a.

In order to compute the Lyapunov spectrum in terms of the parameter a, we have used values in the interval $[0.001, 1.2]$ with $\Delta a = 0.001$. Apart from this, we have also tried to obtain a bifurcation diagram for the variable x_1 in order to reproduce the one in [1]. These results are shown in Fig. 4.1. Note that in the original paper, they do not mention any details on how they did this bifurcation diagram so it was challenging to understand how to obtain this plot. The idea is to search for the maxima of a long time series for several values of the parameter a. In order to this, I managed to compute the derivative of

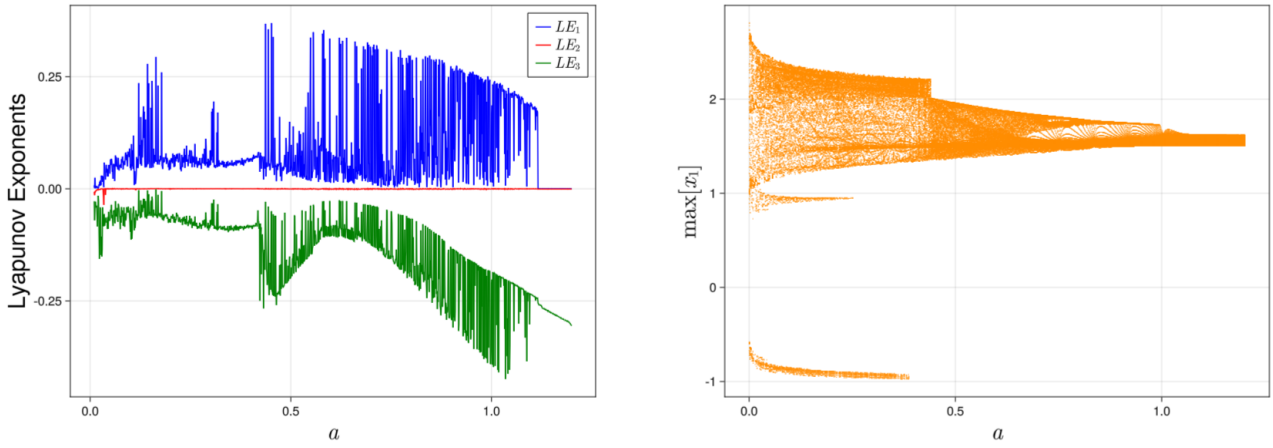

Fig. 4.1. Left Side: Lyapunov Spectrum as a function of the parameter a without the lowest Lyapunov exponent LE_4, since it is larger than the others in absolute value, making the visualization of the rest difficult. **Right Side**: Bifurcation Diagram of x_1 as a function of the parameter a. This is obtained by searching for maxima over a long time series (300 time units in this case).

each variable for all time steps and identify points where the change in sign goes from positive to negative. To obtain a more precise value for the maxima, I utilized a polynomial fit around these points. Eventually, I found a function that performs this task in [19], which I will be using. An example of the maxima found for a concrete time series of x_1 is shown in Fig. 4.2. I I will use the same interval and discretization for a as for the Lyapunov spectrum. Note that in [1], there are not any details about the discretization that is being used.

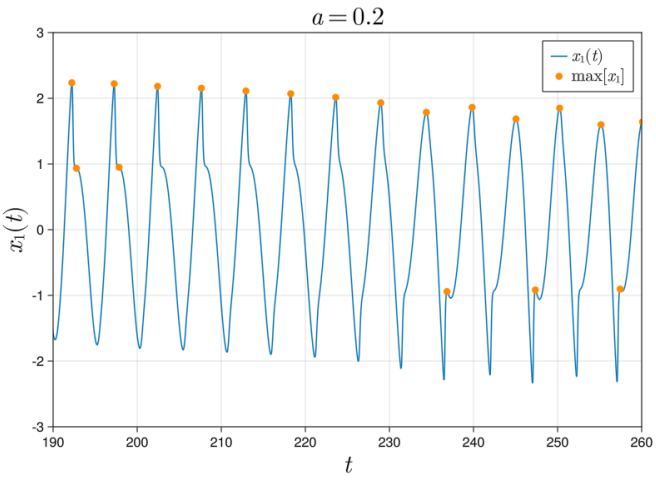

Fig. 4.2. Example of the maxima obtained for the bifurcation diagram for $a = 0.2$ and the rest of the parameters and initial condition are the same as in Sec. 4.1. The orange points are the maxima that is shown in the bifurcation diagram of Fig. 4.1.

From what we can see in Fig. 4.1, the dynamics of the system are quite complicated. In the vast majority of the interval under study, we observe that there is almost always a positive value for the largest Lyapunov exponent. Thus, the behavior is mostly chaotic in this case. Nevertheless, we can identify a quasi-periodic window of behavior for values of a in the range $[1.118, 1.2]$ approximately. This finding is consistent with results in [1]. Note that just by looking at Fig. 4.1, we cannot exactly discern whether the Lyapunov exponent is truly zero since our criterion is that it should be on the order of 10^{-5} or lower to be considered zero.

On the other hand, looking at the bifurcation diagram, we also observe that the distribution of the maxima as a function of a is quite complex. For low values of the parameter (a in the range $[0.01, 0.45]$ approximately), we see that there are different branches that are very far apart from each other, except for the region where there is a very complex distribution of the maxima (x_1 in the range $[1.0, 2.5]$ approximately). As we increase a, the lower branches disappear and we are left with a maxima distribution that starts to shrink, indicating that the maxima tend to be bounded in a smaller range as we increase the parameter.

Additionally to what we have already done, we will also compute a dynamical map by changing the parameters a and b. Thus, for each value of the pair (a, b), we will compute the Lyapunov spectrum and classify its dynamics in terms of the number of positive, zero, or negative exponents using the following criteria: Chaos corresponds to one positive Lyapunov exponent and the rest negative; Hyper-Chaos corresponds to two positive Lyapunov exponents and the rest negative; and Quasi-Periodic corresponds to one or two zero Lyapunov exponents and the rest negative. In order to consider effectively zero the Lyapunov exponent, we will use the criteria previously discussed in Sec. 3. To construct this dynamical map, we will use $a \in [0.01, 1.20]$ and $b \in [0.01, 0.60]$ with $\Delta a = \Delta b = 0.01$. The results of this analysis can be seen in Fig. 4.3. These ranges are the same as those in [1], but the discretization we are using is clearly inferior when comparing the resolution of my plot with the original paper. I have not further improved the discretization since it was very time-consuming.

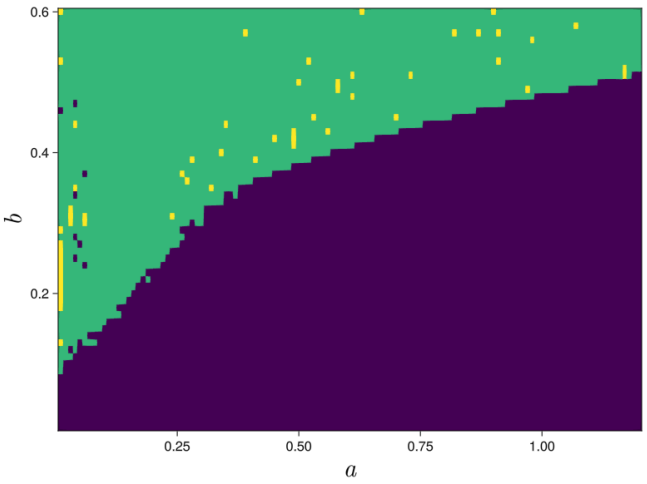

Fig. 4.3. Dynamical Map of the 4D system varying parameters a and b. Yellow, blue, and purple colors correspond to hyper-chaos, chaos, and quasi-periodic behavior in the system respectively.

As can be seen in Fig. 4.3, there appear to be two distinct regions in which we observe chaotic and quasi-periodic behavior. Generally, these two clear regions are consistent with the dynamical map obtained in [1]. However, within the chaotic region, we find some values that seem to exhibit hyper-chaos and also a few small periodic windows. To illustrate these different behaviors, Fig. 4.4 shows the x_1-x_2 projection for several values of the parameters. The initial condition and the rest of the parameters are the same as those that we have been using throughout. In these plots, we present another example of chaotic dynamics for $a = 0.00006$, obtaining similar behavior as in [1]. In the other two plots, we show quasi-periodic motion in which the system tends to approach an almost closed orbit that

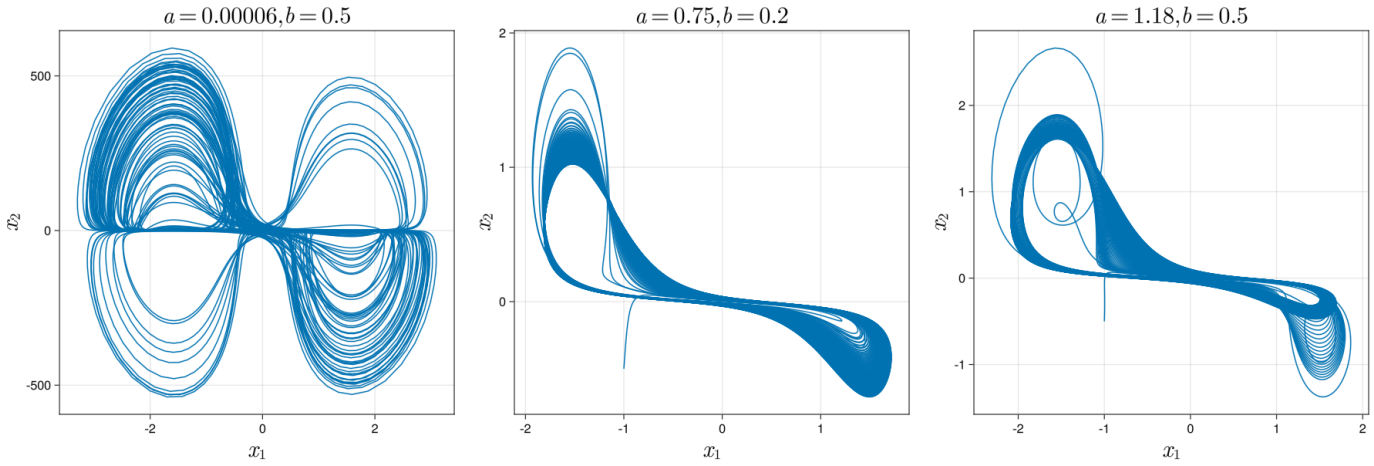

Fig. 4.4. Phase portrait projection of x_1-x_2 for various values of the parameter pair (a, b). The first plot on the left shows chaotic dynamics, while the other two illustrate quasi-periodic behavior.

slightly changes over time. This can be better observed in the video files "x1x2_a1b1.mp4", "x1x2_a2b2.mp4" and "x1x2_a3b3.mp4". In these videos, the evolution of three initial conditions, which are slightly modified versions of the one we previously defined with a small change of 10^{-4}, can be observed. In the video, we can observe how all three slightly different initial conditions exhibit completely different behaviors as time progresses in the chaotic case, while in the quasi-periodic state, we can hardly distinguish them, as their evolution is nearly identical.

4.3. Bursting Phenomena

Bursting is a significant phenomenon in neuroscience where neurons alternate between periods of activity (spiking) and inactivity (resting) while transmitting messages [20]. This behaviour is not exclusive to the brain, it is also observed in various dynamic systems [21], often linked with specific dynamical behaviors such as Hopf and saddle bifurcations as we have seen in the lectures.

The emergence of bursting typically happens in systems with two different timescales. In such systems, faster changes are influenced by slower ones, leading to the rhythmic bursting behavior. Essentially, bursting reflects a dynamic interaction between different time scales within the system, resulting in periodic episodes of activity and rest.

In order to analyze the bursting phenomena in our system, given by Ec. 2.5, we will divide it in two subsystem corresponding to the slow and fast variables which is a usual method to analyze this behaviour [22]. Following what is done in [1], the fast subsystem is

$$\begin{cases} \dot{x}_1 = -\left(a x_2^2 - b\right) x_1 - (\alpha x_4 + \beta) x_3, \\ \dot{x}_3 = x_1, \\ \dot{x}_4 = x_3 \end{cases} \tag{4.5}$$

while the slow subsystem corresponds to

$$\dot{x}_2 = -c x_1 - d x_2 + e x_1^2 x_2 \tag{4.6}$$

For the fast subsystem, the variable x_2 is now considered as a parameter. The fixed points of this subsystem are given by $(0, 0, x_4)\ \forall x_4 \in \mathbb{R}$. The Jacobian of the fast subsystem evaluated at the fixed point is given by

$$J_{fast} = \begin{pmatrix} -\left(a x_2^2 - b\right) & -(\alpha x_4 + \beta) & 0 \\ 1 & 0 & 0 \\ 0 & 1 & 0 \end{pmatrix} \tag{4.7}$$

Therefore, the characteristic equation for obtaining the eigenvalues is described as

$$\lambda \left[\lambda^2 + \left(a x_2^2 - b\right)\lambda + (\alpha x_4 + \beta)\right] = 0. \tag{4.8}$$

Apart from the trivial solution $\lambda_0 = 0$, it is straight forward to obtain

$$\lambda_\pm = \frac{-\left(a x_2^2 - b\right) \pm \sqrt{\left(a x_2^2 - b\right)^2 - 4(\alpha x_4 + \beta)}}{2}. \tag{4.9}$$

Studying the eigenvalues $\lambda_\pm$ and their dependence on the system parameters, we observe the occurrence of a Hopf bifurcation for

$$a x_2^2 - b = 0,\ \alpha x_4 + \beta > 0. \tag{4.10}$$

For these specific values, the real part of $\lambda_\pm$ equals zero, indicating purely imaginary eigenvalues. Consequently, a Hopf bifurcation occurs in this scenario. More concretely, this conditions are satisfied for

$$x_2 = \pm\sqrt{\frac{b}{a}},\ \ x_4 > -\frac{\beta}{\alpha}. \tag{4.11}$$

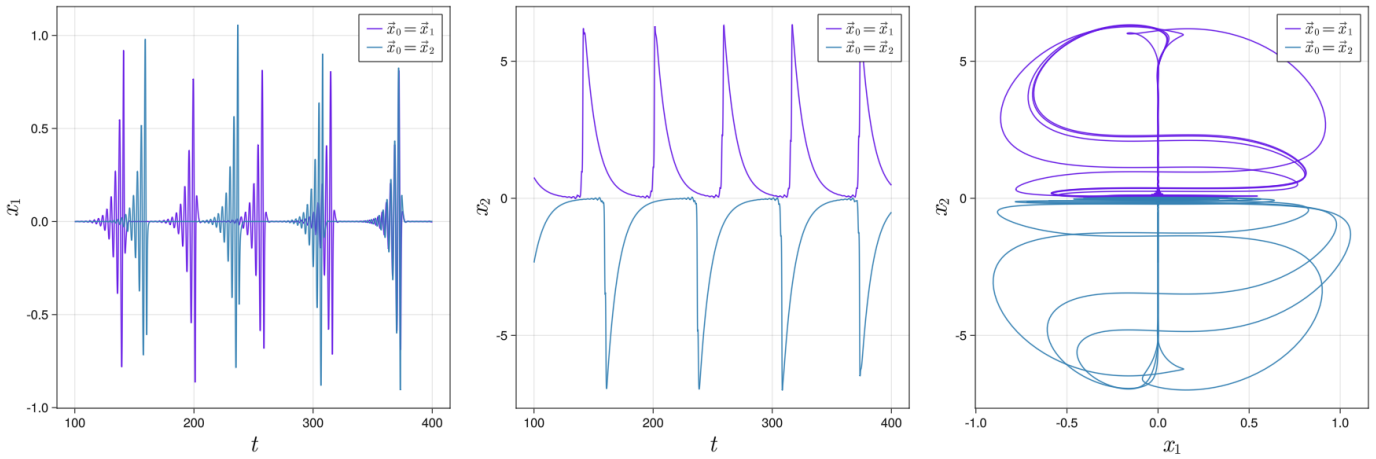

Fig. 4.5. Temporal series of x_1, x_2 and the corresponding x_1-x_2 projection using two different initial conditions $\vec{x}_1 = (0.0, 2.0, 1.0, 0.0)$ and $\vec{x}_2 = (2.0, -1.0, 1.0, 2.0)$.

Thus, depending on the value of x_2, the eigenvalues $\lambda_\pm$ can have a positive or negative value of their real part leading to a stable or unstable focus (at the Hopf bifurcation the real part is zero).

In order to see this behaviour, we are going to be using $a = 0.1$, $b = 0.4$, $c = 0.2$, $d = 0.1$, $e = 4.0$, $\alpha = 0.1$ and $\beta = 3.0$. We will also use two different initial conditions $\vec{x}_1 = (0.0, 2.0, 1.0, 0.0)$ and $\vec{x}_2 = (2.0, -1.0, 1.0, 2.0)$. These are the same parameters and initial conditions that are used in [1].

Results for these simulations are shown in 4.5, in which we can see the bursting behaviour for both initial conditions. Furthermore, we can see two coexisting attractors depending on the initial condition. As the system evolves, x_1 oscillates, its swings getting bigger over time. Once these swings reach a certain size, they trigger a spike in the variable x_2, leading to a bursting phenomenon. This can be seen in the "bursting.mp4" video on the GitHub [2].

Additionally, we can compute the largest Lyapunov exponent obtaining $\mathrm{LE}_1 = 0.0053$ and $\mathrm{LE}_1 = 0.0186$ for the initial conditions $\vec{x}_1$ and $\vec{x}_2$ respectively. This means that the bursting dynamics are also chaotic in this case.

5. CONCLUSIONS

We have investigated the chaotic dynamics of the four-dimensional system described by Eq. 2.5. Specifically, we have successfully replicated the results reported in [1], including the form of the chaotic attractor (Fig. 2.1), the Lyapunov spectrum and bifurcation diagram with variations in the parameter a (Fig. 4.1), and the dynamical map for pairs of parameters (a, b) (Fig. 4.3). During this analysis, we have observed both chaotic and quasi-periodic behavior, as demonstrated in some examples in Fig. 4.4.

Additionally, in Sec. 4.3, we have seen that this system also exhibits bursting behavior when appropriately adjusting the initial conditions and parameters. This behavior can be understood in terms of the fast 3D and slow 1D subsystems present within the 4D system. Specifically, we identified a Hopf bifurcation in the fast 3D system, which leads to the bursting phenomenon. These results were illustrated in Fig. 4.5.

To enhance visualization of the various dynamics discussed in this study, several video files have been created and are available in the "Videos" folder in [2].

REFERENCES

[1] Birong Xu et al. "A memristor–meminductor-based chaotic system with abundant dynamical behaviors". In: *Nonlinear Dynamics* 96 (2019), pp. 765–788.

[2] Daniel D. Montesinos Capacete M.C. *Dynamical Study of a 4D Chaotic System*. Feb. 2024. URL: https://github.com/SrMontesinos01/Dynamical-Systems-Project.

[3] L. Chua. "Memristor-The missing circuit element". In: *IEEE Transactions on Circuit Theory* 18.5 (1971), pp. 507–519. DOI: 10.1109/TCT.1971.1083337.

[4] Leon O Chua and Sung Mo Kang. "Memristive devices and systems". In: *Proceedings of the IEEE* 64.2 (1976), pp. 209–223.

[5] Dmitri B Strukov et al. "The missing memristor found". In: *nature* 453.7191 (2008), pp. 80–83.

[6] Massimiliano Di Ventra, Yuriy V. Pershin, and Leon O. Chua. "Circuit Elements With Memory: Memristors, Memcapacitors, and Meminductors". In: *Proceedings of the IEEE* 97.10 (Oct. 2009), pp. 1717–1724. ISSN: 0018-9219. DOI: 10.1109/jproc.2009.2021077. URL: http://dx.doi.org/10.1109/JPROC.2009.2021077.

[7] Guang-Yi Wang et al. "A flux-controlled model of meminductor and its application in chaotic oscillator". In: *Chinese Physics B* 25.9 (2016), p. 090502.

[8] Y Liang, H Chen, and DS Yu. "A practical implementation of a floating memristor-less meminductor emulator". In: *IEEE Transactions on Circuits and Systems II: Express Briefs* 61.5 (2014), pp. 299–303.

[9] Ying Xu et al. "Synchronization between neurons coupled by memristor". In: *Chaos, Solitons & Fractals* 104 (2017), pp. 435–442.

[10] Ioannis Vourkas and Georgios Ch Sirakoulis. "Emerging memristor-based logic circuit design approaches: A review". In: *IEEE circuits and systems magazine* 16.3 (2016), pp. 15–30.

[11] Ge Zhang et al. “Selection of spatial pattern on resonant network of coupled memristor and Josephson junction”. In: *Communications in Nonlinear Science and Numerical Simulation* 65 (2018), pp. 79–90.

[12] Ge Zhang et al. “Investigation of dynamical behaviors of neurons driven by memristive synapse”. In: *Chaos, Solitons & Fractals* 108 (2018), pp. 15–24.

[13] Shiping Wen et al. “Memristive fully convolutional network: An accurate hardware image-segmentor in deep learning”. In: *IEEE Transactions on Emerging Topics in Computational Intelligence* 2.5 (2018), pp. 324–334.

[14] Shiping Wen et al. “Memristor-based echo state network with online least mean square”. In: *IEEE Transactions on Systems, Man, and Cybernetics: Systems* 49.9 (2018), pp. 1787–1796.

[15] George Datseris. “DynamicalSystems.jl: A Julia software library for chaos and nonlinear dynamics”. In: *Journal of Open Source Software* 3.23 (Mar. 2018), p. 598. DOI: 10.21105/joss.00598. URL: https://doi.org/10.21105/joss.00598.

[16] Christopher Rackauckas and Qing Nie. “DifferentialEquations.jl–a performant and feature-rich ecosystem for solving differential equations in Julia”. In: *Journal of Open Research Software* 5.1 (2017).

[17] Ch Tsitouras. “Runge–Kutta pairs of order 5 (4) satisfying only the first column simplifying assumption”. In: *Computers & Mathematics with Applications* 62.2 (2011), pp. 770–775.

[18] George Datseris and Ulrich Parlitz. *Nonlinear dynamics: a concise introduction interlaced with code*. Springer Nature, 2022.

[19] John F. Gibson. *How to find the local extrema of the solutions when solving a differential equation*. Forum post on Discourse. University of New Hampshire. 2024. URL: https://discourse.julialang.org/t/how-to-find-the-local-extrema-of-the-solutions-when-solving-a-differential-equation/94628/12.

[20] M Deschenes, JP Roy, and M Steriade. “Thalamic bursting mechanism: an inward slow current revealed by membrane hyperpolarization”. In: *Brain research* 239.1 (1982), pp. 289–293.

[21] Huagan Wu et al. “Chaotic and periodic bursting phenomena in a memristive Wien-bridge oscillator”. In: *Nonlinear Dynamics* 83 (2016), pp. 893–903.

[22] Wondimu Teka, Joël Tabak, and Richard Bertram. “The relationship between two fast/slow analysis techniques for bursting oscillations”. In: *Chaos: An Interdisciplinary Journal of Nonlinear Science* 22.4 (2012).

[23] Shiping Wen et al. “General memristor with applications in multilayer neural networks”. In: *Neural Networks* 103 (2018), pp. 142–149.